IOP Publishing Journal of Physics: Condensed Matter
J. Phys.: Condens. Matter **26** (2014) 185006 (9pp) doi:10.1088/0953-8984/26/18/185006

Exciton diffusion in disordered small molecules for organic photovoltaics: insights from first-principles simulations

Z Li, X Zhang and G Lu

Department of Physics and Astronomy, California State University Northridge, CA 91330, USA

E-mail: ganglu@csun.edu

Received 16 January 2014, revised 5 March 2014
Accepted for publication 12 March 2014
Published 22 April 2014

Abstract

Exciton diffusion in small molecules 3,6-bis(5-(benzofuran-2-yl)thiophen-2-yl)-2,5-bis (2-ethylhexyl)pyrrolo[3,4-c]pyrrole-1,4-dione [DPP(TBFu)$_2$] is studied using first-principles simulations. We have examined dependence of exciton diffusion on structure disorder, temperature and exciton energy. We find that exciton diffusion length and diffusivity increase with structural order, temperature and the initial exciton energy. Compared to conjugated polymer poly(3-hexylthiophene) (P3HT), DPP(TBFu)$_2$ small molecules exhibit a much higher exciton diffusivity, but a shorter lifetime. The exciton diffusion length in DPP(TBFu)$_2$ is 50% longer than that in P3HT, yielding a higher exciton harvesting efficiency; the physical origin behind these differences is discussed. The time evolutions of exciton energy, electron-hole distance, and exciton localization are explored, and the widely speculated exciton diffusion mechanism is confirmed theoretically. The connection between exciton diffusion and carrier mobilities is also studied. Finally we point out the possibility to estimate exciton diffusivity by measuring carrier mobilities under AC electric fields.

Keywords: exciton, diffusion, small molecules, organic photovoltaics, first-principles, molecular dynamics

S Online supplementary data available from (stacks.iop.org/JPhysCM/26/185006/mmedia)

(Some figures may appear in colour only in the online journal)

1. Introduction

Over the past decade, tremendous effort has been devoted to the development of organic photovoltaics (OPVs). In particular, the OPVs based on bulk heterojunctions consisting of p-type polymer donors and n-type fullerene derivative acceptors have been the focus of research effort [1, 2]. More recently, solution-processed small molecules are showing great promise as donor materials in OPVs [3–6] whose power conversion efficiency (PCE) has exceeded 7% [6]. These small molecules offer some important advantages over the polymers, including facile synthesis and purification, higher tendency of self-assembly into ordered domains, and freedom from undesirable batch-to-batch variations and end-group contaminations.

Exciton diffusion is crucial to the performance of OPVs because excitons have to migrate to the donor/acceptor interfaces for charge separation within their lifetimes. The average distance that an exciton can travel to during its lifetime is called exciton diffusion length L_D, which is one of the key material parameters that determine the internal quantum efficiency of OPVs. There exist a number of experimental approaches which can estimate L_D, including the measurements of exciton–exciton annihilation [7–9], microwave conductivity [10, 11], heterojunction photocurrent [12–14], and photoluminescence quenching [15–21]. Unfortunately, since there is no universally accepted method for measuring L_D, different L_D values for the same material are typically reported as the result of using different experimental approaches. Even when the same experimental approach (such as the

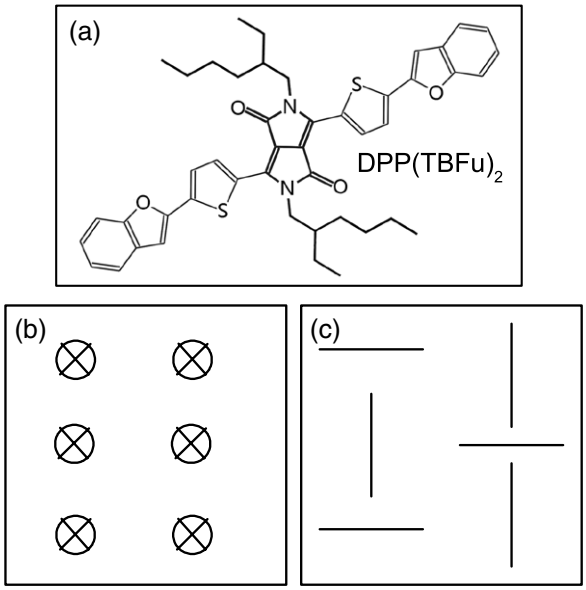

Figure 1. (*a*) The atomic/chemical structure of the $DPP(TBFu)_2$ molecule. (*b*) and (*c*) schematically display the molecular packing of the disordered structure I and II, respectively; each ⊗ or — represents the backbone of the $DPP(TBFu)_2$ molecule.

popular photoluminescence quenching) is used, many challenges remain for an accurate experimental determination of L_D. For instance, well-characterized donor/acceptor interfaces may be required [17] and optical interference has to be eliminated [18] to name just a few. In addition to the experimental challenges, there is a lack of clear understanding of exciton diffusion mechanism; in particular, the material parameters and physical factors that govern exciton diffusion still elude us. Such understanding is important for the formulation of materials design rules which could ultimately be used to reduce the time and labor in developing novel materials with higher L_D, thus allowing for larger domain sizes and more efficient carrier generation in OPVs.

In this paper, we carry out first-principles simulations to study exciton diffusion in disordered small molecules 3,6-bis(5-(benzofuran-2-yl)thiophen-2-yl)-2,5-bis(2-ethylhexyl)pyrrolo[3,4-c]pyrrole-1,4-dione [$DPP(TBFu)_2$]. The small molecules $DPP(TBFu)_2$ whose chemical structure is shown in figure 1(*a*) have been used as donor material in bulk heterojunction OPVs with a PCE of 4.4% [22]. The exciton diffusion length, lifetime, diffusivity and harvesting efficiency in the disordered $DPP(TBFu)_2$ molecules are determined for two different structural disorders and at different temperatures. The first-principles simulations provide a means to estimate L_D at a quantum chemical level, offer insights into the exciton diffusion process and shed light on the physical factors governing exciton diffusion. It is hoped that such first-principles study could be a worthy partner to the experiments and pave the way for computational design of more efficient OPVs.

2. Computation method and molecular structure

Exciton diffusion in organic materials has been studied theoretically by using a Forster-type energy transfer model; the previous work determined exciton transition rates based on either an empirical Miller–Abrahams form [23, 24] or quantum chemical calculations [25–27]. Although very powerful in dealing with molecular crystals, these approaches are generally not applicable to amorphous materials such as disordered small molecules as examined in this work. We have recently developed an efficient first-principles method that can predict exciton diffusion behavior in disordered semiconductors [28]. The method consists of three components including: (1) *ab initio* Born–Oppenheimer molecular dynamics (BOMD) simulations using time-dependent density functional theory (TDDFT) [29, 30] with a range-separated exchange-correlation (XC) functional [31–35] for determining exciton energies and many-body wave-functions; (2) non-adiabatic molecular dynamics (NAMD) [36–39] for evaluating phonon-assisted transition rates between the many-body exciton states, and (3) Monte Carlo (MC) calculations for simulating the exciton diffusion process. Since the technical details of the method have been reported elsewhere [28], we shall minimize the discussion of the method in this paper and focus primarily on the simulation results from the method.

The exciton diffusion is modeled in a molecular system comprised of 33 × 33 × 33 (= 35937) simulation boxes, and the lattice constant of each cubic box is 19.0 Å. The BOMD simulation is performed in one of the 35 937 cubes, referred to as the home cube, whose electronic wave-functions and energies are determined from BOMD to generate the wave-functions and energetic disorder of the entire disordered system. More specifically, the exciton wave-functions and energies in the home cube are calculated based on Casida's formulation of TDDFT [29] at each BOMD time-step. The wave-functions in each of the remaining cubes are randomly selected from those of the home cube at a different BOMD snapshot and they are then randomly rotated before being assigned to each cube. This is an approximate scheme to produce the wave-function network that resembles the true wave-functions of the entire disordered system (which otherwise are impossible to calculate). The justification and validation of this scheme can be found elsewhere [28]. The NAMD simulation is subsequently carried out for the home cube to determine the phonon-assisted transition rates between these exciton states (see Appendix A for details) [28, 40]; the spontaneous emission rates are estimated by using the transition dipole moment approximation. The total transition rates are the sum of these two rates. Based on the transition rates, MC simulations are carried out for 100 different molecular conformations and 100 exciton diffusion trajectories for each of the molecular conformations; the exciton diffusion length and lifetime are then averaged out over these 10^4 MC trajectories (see Appendix B for details).

Since the molecular structure is not well characterized in disordered $DPP(TBFu)_2$ films, here we assume that the disordered molecular structure comprises of both herringbone and cofacial motifs, accompanied by random translations and rotations of the backbones. To model such structures, we construct the home cube with six $DPP(TBFu)_2$ molecules (612 atoms) arranged differently to generate two representative structures as shown in figures 1(*b*) and (*c*). In structure I, we align the

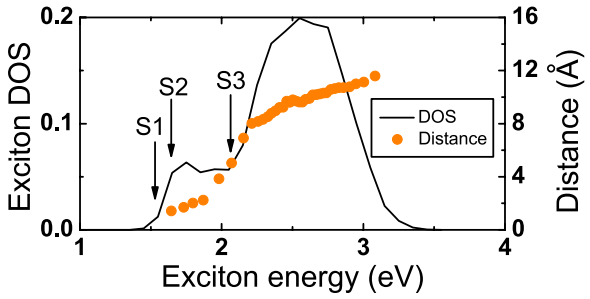

Figure 2. The exciton density of states in the home cube at 300 K. The arrow indicates the energy position of S1, S2, and S3 exciton states. The orange dots represent the electron-hole distance for each exciton state averaged over the BOMD configurations.

molecular backbones along the same direction to resemble the cofacial packing, while in structure II, the neighboring backbones are orientated perpendicularly to each other, similar to the herringbone packing. Subject to the subsequent molecular dynamics simulations, the molecules in the home cube can shift and rotate relative to each other. In an earlier work, we have established quantitatively that structure II is more disordered than structure I by examining local deformation and wave-function localization length [41]. We believe that the simulations of these two representative structures could capture the essential physics of exciton diffusion in disordered DPP(TBFu)$_2$ films. A more detailed description of the computational parameters is summarized in Appendices C and D.

3. Results and discussion

First, we have determined the density of states (DOS) of excitons in structure II at 300 K and the result is shown in figure 2. DOS at a given energy interval represents the number of possible exciton states due to different atomic configurations over the course of the BOMD simulation. Also displayed in the figure is the electron-hole distance (orange dots) as a function of exciton energy. The electron-hole distance is calculated based on the position of the quasi-electron and quasi-hole from the exciton many-body wave-functions [28]. There are two peaks in DOS with the lower one corresponding to the intra-molecular excitons because of the smaller electron-hole distances. These intra-molecular excitons are the predominant product of photo-excitation, hence they are the focus of the present study. Since exciton diffusion depends on the initial energy of the exciton, we will examine three representative initial states labeled as S1, S2, and S3 of the intra-molecular excitons in the following.

The simulation results of exciton diffusion are summarized in table 1. The diffusion length L_D and lifetime τ are averaged from the MC simulations over 10^4 trajectories; the diffusivity D is evaluated as $D = < L^2 >/\tau$, where L is the diffusion distance for a specific MC trajectory, and $< ... >$ indicates the average over MC trajectories. We find that the diffusion length of structure II ranges from 8.3 nm to 11.4 nm, in an excellent agreement with the experimental value of 8.7 nm for as-cast films of C_6PT_2-DPP(TBFu)$_2$ molecules [42]. C_6PT_2-DPP(TBFu)$_2$ molecules have the identical core as DPP(TBFu)$_2$ but with slightly different side-groups.

Table 1. Simulated exciton diffusion length L_D (nm), lifetime τ (ns), and diffusivity D (10^{-8} m^2 s^{-1}) for S1, S2, and S3 at 300 K.

	Structure I			Structure II		
	S1	S2	S3	S1	S2	S3
L_D	11.5	12.3	13.6	8.3	10.1	11.4
τ	0.51	0.50	0.50	0.56	0.55	0.54
D	37.3	42.7	47.6	19.1	25.8	30.7

Exciton diffuses by hopping from one localized excited state to another, hence its diffusivity is determined by the transition rates between the localized excited states; the transition rates in turn depend on the intrinsic phonon-assisted transition rates and the energetic disorder (i.e. the energy barriers for exciton hopping) [28, 41]. In general, the intrinsic transition rates, determined by the overlap between the many-body exciton wave-functions in the presence of thermal fluctuations, are of similar order of magnitude among organic semiconductors because of their common π–π stacking. Hence, the primary difference in the exciton transition rates among different organic materials is reflected by their energetic disorder: a larger energetic disorder would lead to smaller exciton transition rates and a lower exciton diffusivity. From table 1, we find that the exciton diffusion length and diffusivity of the structure I are larger than those of structure II since the former is less disordered than the latter [43–45]. For both structures, we observe that the diffusion length and diffusivity increase with temperature and initial exciton energy; the same trend has also been found in the conjugated polymer P3HT [28]. More specifically, the diffusion length and diffusivity of S2 exciton in structure II at 100 K are 7.9 nm and 4.2 × 10^{-8} m^2 s^{-1}, respectively, both lower than the corresponding value at 300 K. The exciton lifetime in structures I and II (∼ 0.5 ns) is in the same order of magnitude as the experimental value for C_6PT_2-DPP(TBFu)$_2$ molecules (∼ 2.4 ns). The exciton lifetime at 100 K (2.0 ns) is longer than that at 300 K because of the lower phonon-assisted annihilation rates at 100 K. Compared to P3HT, the exciton diffusivity in DPP(TBFu)$_2$ is one order of magnitude higher (e.g. $D = 2.1 \times 10^{-8}$ m^2 s^{-1} for P3HT at 300 K) [28]. This is due to the fact that (1) in P3HT, each thiophene ring can rotate relative to its neighbor rings, rendering more flexible molecular structures and larger energy fluctuations in P3HT [46, 47] while in DPP(TBFu)$_2$, the DPP(TBFu)$_2$ core is much less flexible. (2) Unlike P3HT polymers which could take different conjugation lengths, the small DPP(TBFu)$_2$ molecules have identical structure units, hence a more uniform energy distribution (or less energetic disorder) than P3HT.

The exciton lifetime in P3HT is ∼2.4 ns which is four times longer than that in DPP(TBFu)$_2$. This is because the phonon-assisted annihilation rates in DPP(TBFu)$_2$, spanning from 10^8 to 10^{10} s^{-1}, are one order of magnitude higher than those in P3HT (the phonon-assisted annihilation rates dominate the spontaneous annihilation rates in both materials). The distinctive annihilation rates between P3HT and DPP(TBFu)$_2$ are due to their different excitation energies. The lowest excitation energy (the energy difference between the first excited state and the ground state) is 1.7 eV for DPP(TBFu)$_2$ and

Table 2. Exciton harvesting efficiency (%) for the $DPP(TBFu)_2$ layer with two different thicknesses. Both structure I and II are examined for S2 and S3 initial states. The harvesting efficiency of P3HT is also listed for comparison.

	Structure I		Structure II		P3HT
	S2	S3	S2	S3	S3
10 nm	81	89	76	84	70
70 nm	18	19	14	16	10

2.6 eV for P3HT. The lower the excitation energy, the higher the exciton annihilation rates, and the shorter the lifetime. The experimental value for the lowest excitation energy is 1.8 eV for $DPP(TBFu)_2$ and 2.85 eV for oligothiophene with 6 rings [48] which is similar to disordered P3HT. Finally the exciton diffusion length in $DPP(TBFu)_2$ is 10.1 nm, 1.6 times longer than that in P3HT (6.4 nm).

We have calculated exciton diffusion distances along each of 10^4 MC trajectories, and from which we can estimate the exciton harvesting efficiency for a planar donor-acceptor heterojunction (see Appendix B for details). We assume that excitons are generated uniformly in the $DPP(TBFu)_2$ donor layer and they will be harvested as long as they reach the interface. The exciton harvesting efficiency is estimated as $\int_0^{d_0} p(r)\mathrm{d}r/d_0$, where d_0 is the thickness of the $DPP(TBFu)_2$ layer and r is the distance of the exciton from the donor-acceptor interface. $p(r)$ represents the probability that an exciton at r can be harvested, i.e. the probability that the exciton diffusion distance is larger than r. The harvesting efficiency for two different $DPP(TBFu)_2$ layer thicknesses is listed in table 2, and for comparison, we also include the corresponding quantity for P3HT [28]. We find that the harvesting efficiency is larger for the more ordered structure, i.e. the one with the lower thickness of $DPP(TBFu)_2$ layer and excitons with higher initial energies. The fact that the harvesting efficiency in $DPP(TBFu)_2$ is higher than that in P3HT is consistent with the trend of diffusion length between $DPP(TBFu)_2$ and P3HT.

Next we examine exciton dynamics for structure II at 300 K. In figure 3(*a*), we present exciton energy evolution as a function of time. For S1 exciton, the energy variation is essentially flat. In contrast, the energy evolution for S2 and S3 excitons shows a two-step process: when $t < 100$ ps, the energy drops sharply as a function of time but after 100 ps, the energy remains approximately the same. This two-step process is consistent with the experimental observations [15, 49, 50]: exciton diffusion proceeds with an initial downhill migration towards lower energies followed by a thermally activated migration with little energy variation. During the second step, the exciton energy can either increase or decrease, but its average energy is about the same. For S3 exciton, it takes 4 ps for its energy to drop to the initial energy of S2 exciton, indicated by the dashed line in figure 3(*a*), and it takes 108 ps to approach the equilibrium energy of S1 exciton. At 100 K (curves not shown), the two corresponding timescales becomes 8 ps and 187 ps, doubling the timescale at 300 K thanks to the weaker electron–phonon coupling at 100 K. Experimentally, the initial downhill process takes place within a few ps, similar to the computed timescale from S3 to S2.

During exciton diffusion, the exciton may exhibit either an intra-molecular or inter-molecular character. Figure 4(*a*) displays an intra-molecular exciton where the quasi-electron and the quasi-hole are localized on the same molecule. Figure 4(*b*) shows an inter-molecular or charge-transfer exciton where the quasi-electron and the quasi-hole are separated onto different molecules. The greater electron-hole distance in the inter-molecular exciton renders a weaker Coulomb interaction, and hence a higher excitation energy as compared to the intra-molecular exciton. Indeed, the energy of the intra-molecular exciton is found to be 1.65 eV, lower than that of the inter-molecular exciton (2.04 eV). To examine the occupation of these exciton states during diffusion, in figure 3(*b*) we plot the electron-hole distance as a function of time for structure II at 300 K. We find that the electron-hole distance for S1 and S2 is less than 2 Å during the diffusion process, indicating that S1 and S2 are primarily intra-molecular excitons. On the other hand, the electron-hole distance of S3 is initially 4.5 Å, which then decreases to less than 2 Å in a few ps, implying that S3 may be a charge-transfer exciton initially, and then evolves to an intra-molecular exciton. This can be understood by the fact that during exciton diffusion, the energy of S3 exciton decreases in time (the energetic downhill migration); this decrease in energy is accompanied with a reduction of the electron-hole distance (i.e. a transition from a charge-transfer exciton to an intra-molecular exciton). Note that the electron-hole distance of ∼2.0 Å after the downhill migration is an average over many MC trajectories, and different exciton trajectories may exhibit different electron-hole distances.

In figure 3(*c*), we examine exciton delocalization as a function of time. Here, we characterize the extent of exciton delocalization by the number (N_m) of $DPP(TBFu)_2$ molecules that the quasi-electron wave-functions extend to during exciton diffusion. N_m can be estimated by $\left(\sum_i p_i^2\right)^{-1}$ where p_i is the quasi-electron population on a molecule i. N_m for the quasi-hole displays similar behavior and thus is not shown here. For S1 and S2, N_m is 1.5 and has small variations during exciton diffusion. This suggests that approximately one-half of the excitons are delocalized onto two molecules and the other half are localized on one molecule only. N_m of S3 is 1.8 initially and then decreases to 1.5 after 100 ps.

In figure 3(*d*), we display the energy variation of S3 exciton (ΔE) as a function of diffusion distance by considering 10^4 MC trajectories for structure II at 300 K. Each data point in the figure corresponds to a MC snapshot whose energy and diffusion distance are shown in the plot. A positive (negative) ΔE represents an energy loss (gain) of the exciton. Therefore the initial downhill migration from S3 to S2 is approximately indicated by the blue color ($t < 10$ ps) with the positive ΔE, while the thermally activated migration is shown by the black color ($t > 100$ ps) with oscillating ΔE across the zero energy. The red color (10–100 ps) corresponds to an intermediate, where the exciton energy decreases only slightly (from S2 to S1) and the thermally activated migration is also present. The initial downhill migration from S3 to S2 is characterized by

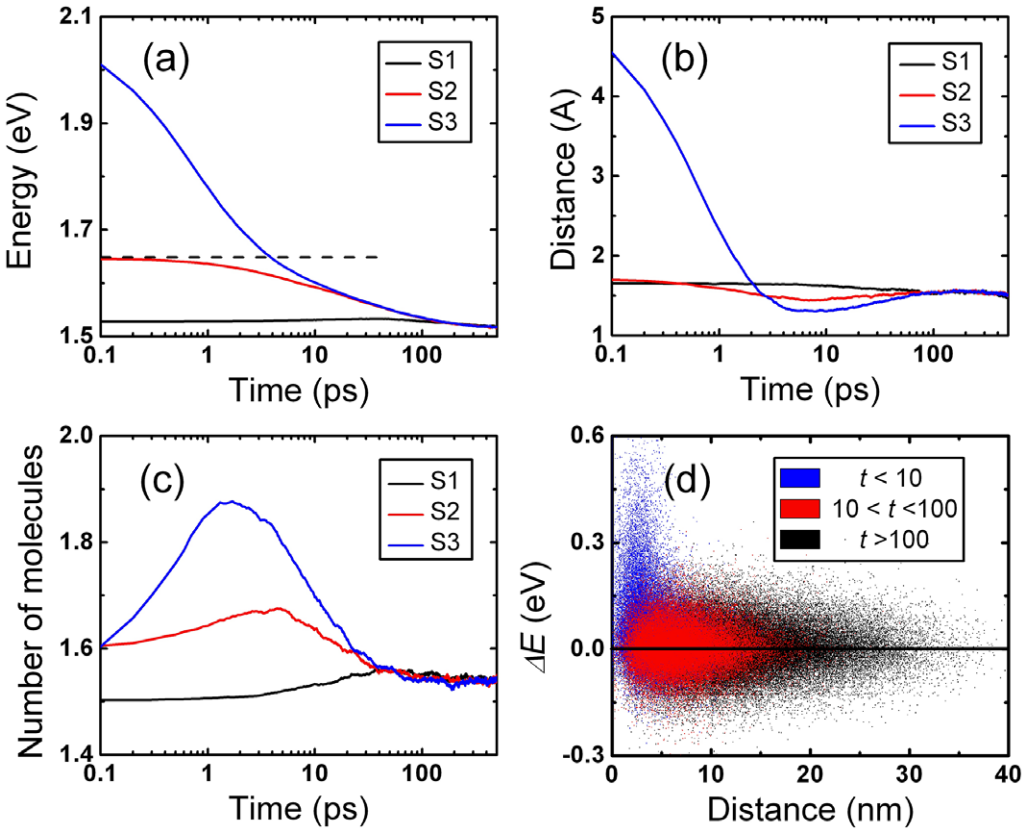

Figure 3. The time evolution in structure II of (*a*) exciton energy, (*b*) electron-hole distance, and (*c*) the number of molecules that the quasi-electron state extends to. The black, red, and blue curves correspond to excitons S1, S2, and S3, respectively. The dashed line in (*a*) indicates the initial energy of the S2 exciton. (*d*) The variation of exciton energy versus diffusion distance for the S3 exciton. The color-coding in (*d*) represents different timescales given in ps. The results shown here are obtained from averaging 10^4 MC trajectories.

smaller diffusion distances (∼ 5 nm) but with a greater energy loss (∼ 0.4 eV); in contrast, the thermally activated migration contributes to much longer diffusion distances (up to 30 nm) but with smaller energy variations (±0.2 eV). Note that the diffusion length of 11.4 nm in table 1 is only an averaged value, and the diffusion distances along different MC trajectories can range from 0 to 30 nm (0 means that the exciton is trapped at the original site). At 100 K (figure not shown), the energy variation during the thermally activated process is only 0.05 eV and the process is largely suppressed, leading to a smaller exciton diffusion length than that at 300 K. For P3HT, the initial downhill migration at 300 K exhibits the similar timescale (∼ 10 ns) and diffusion distance (∼ 5 nm) as $DPP(TBFu)_2$ [28], demonstrating that the downhill process does not depend sensitively on materials. This is because during the downhill migration, it is easier for an exciton to find lower energy states to hop to, thus it is essentially independent of the width of exciton DOS. On the other hand, for thermally activated migration, the number of available states for the exciton to hop to plays a crucial role in exciton diffusion—the wider the DOS distribution, the higher the hopping energy barriers, and the lower the transition rates. Therefore, the wider DOS in P3HT due to the greater static and dynamic disorder results in a less efficient thermally activated migration and hence shorter diffusion distances in P3HT (∼ 15 nm) than $DPP(TBFu)_2$ (∼ 30 nm).

For the more ordered structure I, the corresponding exciton diffusion dynamics is shown in figures S1(*a*)–(*d*) in the supplementary information (stacks.iop.org/JPhysCM/26/185006/mmedia). Most of our discussions on figure 3 for structure II apply to structure I as well. Because of higher order, S2 and S3 excitons are more delocalized at the beginning of the diffusion process as shown in figure S1(*c*). In addition, as displayed in figure S1(*d*), the red and black regions extend to longer distances compared to figure 3(*d*).

Since an exciton is a bound quasi-electron and quasi-hole pair, one can gain some insight of exciton diffusion by examining the diffusion of the quasi-electron and quasi-hole separately. The diffusion of the carriers (electrons or holes) can be modeled in a similar manner as excitons except that the KS eigenvalues and eigenstates are used instead of the many-body exciton energies and wave-functions to determine the relevant transition rates [51]. Here we focus on structure II at 300 K and assume that the diffusion time of the carriers is the same as the lifetime of the relevant exciton (e.g. 0.55 ns for S2 exciton). The computed carrier diffusion length and diffusivity are listed in table 3. We find that diffusivity of the quasi-electron and the quasi-hole is 39.4×10^{-8} m^2 s^{-1} and 11.6×10^{-8} m^2 s^{-1}, respectively, while the corresponding exciton diffusivity is in-between them at 25.8×10^{-8} m^2 s^{-1}. Therefore the exciton diffusion can be thought of roughly as an average of the faster electron diffusion and the slower hole

Table 3. The electron and hole diffusion length L_D (nm) and diffusivity D (10^{-8} m^2 s^{-1}) at 300 K for structure II during the lifetime of the S2 exciton. The corresponding values for the S2 exciton are also shown for comparison.

	Hole	Electron	Exciton
L_D	6.8	12.8	10.1
D	11.6	39.4	25.8

diffusion. Since the carrier diffusivity is proportional to carrier mobility via the Einstein relation, one may be able to estimate the exciton diffusivity (or even exciton diffusion length) from a knowledge of carrier mobilities.

In an earlier work, we have determined the zero-field mobility of holes in DPP(TBFu)$_2$ as 3.1×10^{-4} cm^2/(Vs) for structure II at 300 K [41]. According to the Einstein relation, we can estimate the hole diffusivity D as [52]

$$\mu = \frac{e}{k_B T} D, \tag{1}$$

where e is electron charge. Thus mobility of 3.1×10^{-4} cm^2/(Vs) corresponds to diffusivity of 0.08×10^{-8} m^2 s^{-1}, which is much smaller than the hole diffusivity of 11.6×10^{-8} m^2 s^{-1} as shown in table 3. This is because in the carrier mobility calculations, the timescale for carrier diffusion is ~1000 ns and the diffusion distance could be as large as the dimension of the sample, in the order of a few hundred nm. The longer the diffusion distance, the higher the probability that carriers may encounter deep traps, resulting in a lower carrier diffusivity. By assuming that the carrier can only diffuse within the lifetime of the exciton, the diffusion distance becomes ~10 nm. On the other hand, if we let the hole diffuse for 1000 ns, its diffusivity would be 0.19×10^{-8} m^2 s^{-1}, which is much closer to the value (0.08×10^{-8} m^2 s^{-1}) obtained from the carrier mobility calculations. In the same vein, although the mobility difference between structure I and II is 20-fold [41], the diffusivity difference between them is only two-fold; this is because an exciton diffuses a much shorter distance than a hole, hence the effect of structural disorder is smaller on exciton diffusion than on hole mobility. Lastly, we comment on the experimental observation that the carrier mobility under an alternating current (AC) electric field increases with the AC frequency. This is because the higher the frequency, the shorter the diffusion distance; thus the probability that the carrier is trapped is lower and the carrier mobility is higher [53–55]. This observation suggests that the experimental mobility measurements under a direct current (DC) electric field may not provide a reasonable estimate of exciton diffusivity. On the other hand, the AC mobility measurements at a frequency of ~1 GHz, corresponding to the timescale of 1 ns, could provide a reasonable estimate for exciton diffusivity.

4. Conclusion

In summary, we have studied exciton diffusion in disordered small molecules DPP(TBFu)$_2$ using first-principles simulations. The exciton diffusion length, lifetime, diffusivity, and harvesting efficiency are determined, which compare very well to the experimental results on similar DPP(TBFu)$_2$ molecules.

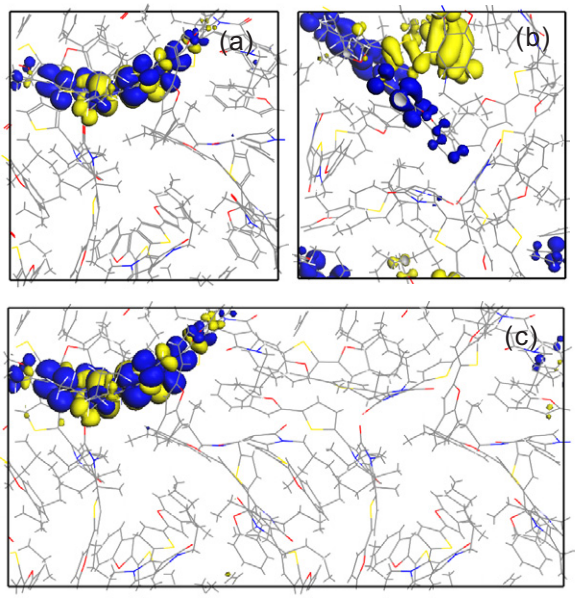

Figure 4. (*a*) Charge density of a typical intra-molecular exciton; (*b*) charge density of a typical charge-transfer exciton; (*c*) the same exciton state as in (*a*) but calculated with a home box that is as twice as large as in (*a*). In each figure, the blue (yellow) isosurface illustrates the charge density distribution at +(−) 0.003 Å^3. The positive (negative) charge density corresponds to the quasi-electron (hole).

The dependence of exciton diffusion on structure disorder, temperature and exciton energy is analyzed. We find that exciton diffusion length and diffusivity increase with the structural order, temperature and the initial exciton energy. Compared to the conjugated polymer P3HT, DPP(TBFu)$_2$ exhibits a much higher exciton diffusivity but a shorter lifetime. The exciton diffusion length in DPP(TBFu)$_2$ is 50% longer than P3HT, yielding a higher exciton harvesting efficiency in DPP(TBFu)$_2$. The time evolutions of exciton energy, electron-hole distance, and exciton localization are examined, and the widely speculated exciton diffusion mechanism, namely an initial downhill migration followed by a thermally activated migration, is confirmed from first-principles. We find that the initial downhill migration takes place in the first ~10 ps and contributes to 5 nm of diffusion distance in DPP(TBFu)$_2$. The thermally activated migration takes over after 100 ps and contributes to a diffusion distance up to 30 nm. During the downhill migration ($t < 10$ ps), the exciton exhibits higher energies, larger electron-hole distances and more extended charge distribution than the thermally activated process. The connection between exciton diffusion and carrier mobilities is also studied. The exciton diffusivity is found to be an average of that of the quasi-electron and the quasi-hole within the lifetime of the exciton (~ 1 ns). Finally we suggest the experimental possibility to estimate exciton diffusivity by measuring carrier mobilities under AC fields.

Acknowledgments

This work was supported by National Science Foundation (DMR-1035480 and DMR-1205734) and the Department of Defense (W911NF-13-1-0147).

Appendix A. Phonon-assisted transition rates from NAMD

During a molecular dynamics trajectory, the time-dependent many-body wave-function of the exciton state, $\Psi(t)$, can be expanded by a linear combination of a complete basis set consisting of the adiabatic ground state and the excited states $\Phi_I[\mathbf{R}(t)]$ at the present ionic positions $\mathbf{R}(t)$:

$$\Psi(t) = \sum_{I=0}^{\infty} C_I(t)\Phi_I[\mathbf{R}(t)], \tag{A.1}$$

where $C_I(t)$ is the expansion coefficient. Let the exciton start in a pure state I at $t = 0$, i.e. $\Psi(0) = \Phi_I[\mathbf{R}(0)]$; then the coefficient $C_J(t)$ in equation (A.1) can be labeled as $C_J^{(I)}(t)$ with the initial condition that $C_J^{(I)}(0) = \delta_{I,J}$. At $t > 0$, ions move and $\Psi(t)$ becomes a mixed state. Therefore $|C_J^{(I)}(t)|^2$ represents the probability that the exciton makes a transition from state I to state J during a small time interval of δt (in this case $\delta t = t - 0$). The phonon-assisted exciton transition rate from state I to J, $\gamma_{I,J}^0$ is thus given by

$$\gamma_{I,J}^0 = \left\langle \frac{|C_J^{(I)}(t)|^2}{t} \right\rangle \delta t. \tag{A.2}$$

The average is taken over a short MD trajectory of δt. Here, we use δt = 100 fs to determine the phonon-assisted transition rates. The evolution of $C_J^{(I)}(t)$ can be determined from the non-adiabatic *ab initio* molecular dynamics at each time step. Substituting equation (A.1) into the time-dependent Schrödinger equation, one arrives at the following equation involving the expansion coefficient $C_J(t)$:

$$\frac{\partial}{\partial t} C_J(t) = -\sum_K C_K(t)\left(\frac{i}{\hbar}\omega_K \delta_{JK} + \mathrm{D}_{JK}\right). \tag{A.3}$$

A standard second-order finite-difference method with a time-step of 10^{-3} fs is employed to propagate the coefficient $C_J(t)$. And D_{JK} is the non-adiabatic coupling between two many-body electronic states J and K, and can be determined by the non-adiabatic coupling between the Kohn–Sham wave-functions [28].

Appendix B. Exciton diffusion process from Monte Carlo simulations

Exciton diffusion is modeled in a molecular system comprised of 33 × 33 × 33 (= 35 937) simulation boxes, and the lattice constant of each cubic simulation box is 19.0 Å. The wave-functions in each of the cubes are randomly selected from those of the home cube at a different BOMD snapshot and they are then randomly rotated before being assigned to each cube. The transition rate between two exciton states is the sum of the phonon-assisted transition rate (from the NAMD simulations) and the spontaneous emission rate (estimated by using the transition dipole moment approximation). Based on these transition rates, kinetic Monte Carlo simulations were carried out for 100 different molecular conformations (each corresponds to a random configuration of the molecular system comprised of 35 937 boxes) and 100 exciton diffusion trajectories for each of the molecular conformation. Along each trajectory, exciton diffusion is modeled as a random walk. For diffusion of the exciton I, one can generate an event table with $M + 1$ transition probabilities ($M = 36$ is the number of excitons considered in the simulation): transition probabilities from the exciton I to $M - 1$ neighboring excitons, $P_{1,2,\ldots,M-1} = \gamma_{I,J} \times \Delta t$ with $J = 1, \ldots, I - 1, I + 1, \ldots, M$; annihilation probability, $P_M = \gamma_{I,0} \times \Delta t$; and the probability to remain at the same state I, $P_{M+1} = 1 - (P_1 + P_2 + \ldots + P_M)$. Here, Δt = 10 fs is the time-step of the MC simulations, and $\gamma_{I,J}$ is the transition rate from I to J. With these probabilities, a diffusion trajectory of the exciton I is obtained by executing MC moves until the exciton is annihilated. From the trajectory, one can determine the lifetime t (the number of MC moves multiplied by Δt) and the maximum distance $d_{\max}$ of exciton diffusion for each trajectory. Averaging over all trajectories yields the exciton diffusion length, lifetime, and diffusivity by $L_{\mathrm{D}} = \langle d_{\max} \rangle$, $\tau = \langle t \rangle$, and $\mathrm{D} = \langle d_{\max}^2 \rangle / \tau$, respectively, where the brackets indicate the arithmetic average.

From the 100 × 100 MC trajectories, a distribution function of exciton diffusion distance (a percentage distribution for each diffusion distance) can be obtained. For a given diffusion distance r, the integration of the distribution function from r to ∞ represents the probability $p(r)$ that an exciton can be harvested. Consider a planar heterojunction in which a $\mathrm{DPP(TBFu)_2}$ donor layer is on top of an acceptor material. Let an exciton be formed at distance r from the interface and assume the excitons are generated homogeneously in the $\mathrm{DPP(TBFu)_2}$ layer, the harvesting efficiency can then be estimated as $\int_0^{d_0} p(r)\mathrm{d}r / d_0$, where d_0 is the thickness of the $\mathrm{DPP(TBFu)_2}$ layer.

Appendix C. Computational details

The Isothermal–Isobaric (NPT) classic MD is first performed for the structures shown in figures 1(*b*) and (*c*) at 500 K to obtain the disordered initial configurations for the home cube. This mass density is 1.1 g cm^{-3}, slightly smaller than the experimentally estimated density of 1.3 g cm^{-3} in a single crystalline phase of $\mathrm{DPP(TBFu)_2}$. These initial configurations are then fully relaxed by static *ab initio* calculations before the *ab initio* BOMD simulations are carried out to bring the systems to 300 K with repeated velocity scalings. The *ab initio* calculations are performed for the home cube using the standard plane-wave pseudopotential approach and Generalized Gradient Approximation (GGA) [56] as implemented in the VASP code [57, 58]. The Γ point is sampled and the energy cut-off of the plane-wave basis is 400 eV. Six highest occupied KS orbitals and six lowest unoccupied KS orbitals are included in the Casida formulation to produce 36 exciton states. Finally, a micro-canonical BOMD production run is carried out for 1000 fs with a time-step of 1 fs. We have examined the auto-correlation functions for the highest-occupied-molecular-orbital (HOMO) and the lowest-unoccupied-molecular-orbital

(LUMO) energies during the micro-canonical MD run, and found that the systems are well equilibrated in 1000 fs.

We have carried out extensive tests to ensure that the selected home box is large enough by examining the convergence of energy levels, wave-functions and charge densities. Here as an example, we double the simulation box for the typical intra-molecular exciton from 19.0Å×19.0Å×19.0Å to 38.0Å×19.0Å×19.0Å. The charge density of the exciton in the smaller and larger simulation box is displayed in figures 4(*a*) and (*c*), respectively. We find that the two charge densities are almost the same, indicating that the results from the smaller simulation box are converged. This smaller home box is the one that was actually used throughout the paper for the first-principles calculations.

Although periodic boundary conditions are used in determining the exciton states in the home box, the wave-functions in all other boxes are *not* the periodic images of the home box. Instead, the wave-functions in the other boxes are generated from the wave-functions in the home box at different MD snapshots; these wave-functions are then randomly rotated before placed in these boxes. Therefore, the wave-functions of the entire system is not periodic, but rather a random network.

Appendix D. Determining the range-separation parameter

In Casida's formulation of TDDFT, a range-separated hybrid XC functional [31–35] is used to describe charge-transfer excitations. In this functional, the exchange part consists of a short-range GGA term and a long-range Hartree–Fock (HF) term, achieved by replacing the electron repulsion operator $1/r$ by $[1-\mathrm{erf}(\alpha r)]/r$ and $\mathrm{erf}(\alpha r)/r$, respectively. Here erf(x) is the error function, and α is a range-separation parameter [31–35]. Owing to the computational cost in the HF calculations, it is impractical to compute the exciton energy for a large system (e.g. a few hundred atoms) at each of the few thousands BOMD snapshots. Recently, we have developed an efficient method to carry out TDDFT calculations with the range-separated XC functional based on the plane-wave pseudopotential VASP code [59] at a much lower computational cost. Herein, we use the method to calculate the exciton energy and many-body wave-functions.

We follow the procedure proposed by Stein *et al* [60] to determine the range-separation parameter α from first-principles. More specifically, α is determined by minimizing the energy difference ΔE:

$$\Delta E(\alpha) = \left|\epsilon_H^\alpha(N) + I^\alpha(N)\right| + \left|\epsilon_H^\alpha(N+1) + I^\alpha(N+1)\right|, \quad \text{(D.1)}$$

where $\epsilon_H^\alpha(N)$ is the HOMO of the N electron neutral system per a specific choice of α and $I^\alpha(N)$ represents the energy difference between the ground state energy of N and N-1 electron systems per the same α. All the total energies and eigenvalues are determined from density functional calculations with the range-separated functional for a single $\mathrm{DPP(TBFu)_2}$ molecule. The minimum energy difference $\Delta E(\alpha)$ is achieved with α = 0.276 $\mathrm{Å}^{-1}$ and the lowest excitation energy is 1.7 eV, similar to the experimental value of 1.8 eV.

References

[1] Thompson B C and Frechet J M J 2008 *Angew. Chem. Int. Edn* **47** 58
[2] Brabec C J, Gowrisanker S, Halls J J M, Laird D, Jia S J and Williams S P 2010 *Adv. Mater.* **22** 3839
[3] Xia P F, Feng X J, Lu J P, Tsang S W, Movileanu R, Tao Y and Wong M S 2008 *Adv. Mater.* **20** 4810
[4] Silvestri F, Irwin M D, Beverina L, Facchetti A, Pagani G A and Marks T J 2008 *J. Am. Chem. Soc.* **130** 17640
[5] Rousseau T, Cravino A, Bura T, Ulrich G, Ziessel R and Roncali J 2009 *Chem. Commun.* 1673
[6] Sun Y M, Welch G C, Leong W L, Takacs C J, Bazan G C and Heeger A J 2012 *Nature Mater.* **11** 44
[7] Lewis A J, Ruseckas A, Gaudin O P M, Webster G R, Burn P L and Samuel I D W 2006 *Org. Electron.* **7** 452
[8] Shaw P E, Ruseckas A and Samuel I D W 2008 *Adv. Mater.* **20** 3516
[9] Stevens M A, Silva C, Russell D M and Friend R H 2001 *Phys. Rev.* B **63** 165213
[10] Huijser A, Savenije T J, Meskers S C J, Vermeulen M J W and Siebbeles L D A 2008 *J. Am. Chem. Soc.* **130** 12496
[11] Kroeze J E, Savenije T J, Vermeulen M J W and Warman J M 2003 *J. Phys. Chem.* B **107** 7696
[12] Halls J J M, Pichler K, Friend R H, Moratti S C and Holmes A B 1996 *Appl. Phys. Lett.* **68** 3120
[13] Pettersson L A A, Roman L S and Inganas O 1999 *J. Appl. Phys.* **86** 487
[14] Yoo S, Domercq B and Kippelen B 2004 *Appl. Phys. Lett.* **85** 5427
[15] Mikhnenko O V, Cordella F, Sieval A B, Hummelen J C, Blom P W M and Loi M A 2008 *J. Phys. Chem.* B **112** 11601
[16] Stoessel M *et al* 2000 *J. Appl. Phys.* **87** 4467
[17] Markov D E, Amsterdam E, Blom P W M, Sieval A B and Hummelen J C 2005 *J. Phys. Chem.* A **109** 5266
[18] Scully S R and McGehee M D 2006 *J. Appl. Phys.* **100** 034907
[19] Markov D E, Tanase C, Blom P W M and Wildeman J 2005 *Phys. Rev.* B **72** 045217
[20] Haugeneder A, Neges M, Kallinger C, Spirkl W, Lemmer U, Feldmann J, Scherf U, Harth E, Gügel A and Müllen K 1999 *Phys. Rev.* B **59** 15346
[21] Mani A, Schoonman J and Goossens A 2005 *J. Phys. Chem.* B **109** 4829
[22] Walker B, Tomayo A B, Dang X D, Zalar P, Seo J H, Garcia A, Tantiwiwat M and Nguyen T Q 2009 *Adv. Funct. Mater.* **19** 3063
[23] Meskers S C J, Hubner J, Oestreich M and Bassler H 2001 *J. Phys. Chem.* B **105** 9139
[24] Madigan C and Bulovic V 2006 *Phys. Rev. Lett.* **96** 046404
[25] Bredas J L, Beljonne D, Coropceanu V and Cornil J 2004 *Chem. Rev.* **104** 4971
[26] Hennebicq E *et al* 2005 *J. Am. Chem. Soc.* **127** 4744
[27] Kose M E, Graf P, Kopidakis N, Shaheen S E, Kim K and Rumbles G 2009 *ChemPhysChem* **10** 3285
[28] Zhang X, Li Z and Lu G 2011 *Phys. Rev.* B **84** 235208
[29] Casida M E 1995 *Recent Advances in Density Functional Methods* ed Chong D P (Singapore: World Scientific)
[30] Onida G, Reining L and Rubio A 2002 *Rev. Mod. Phys.* **74** 601
[31] Iikura H, Tsuneda T, Yanai T and Hirao K 2001 *J. Chem. Phys.* **115** 3540
[32] Tawada Y, Tsuneda T, Yanagisawa S, Yanai T and Hirao K 2004 *J. Chem. Phys.* **120** 8425
[33] Karolewski A, Stein T, Baer R and Kummel S 2011 *J. Chem. Phys.* **134** 151101
[34] Wong B M and Hsieh T H 3704 (2010) *J. Chem. Theory Comput.* **6** 3704
[35] Minami T, Nakano M and Castet F 2011 *J. Phys. Chem. Lett.* **2** 1725

[36] Li Z, Zhang X and Lu G 2010 *J. Phys. Chem.* B **114** 17077
[37] Duncan W R, Stier W M and Prezhdo O V 2005 *J. Am. Chem. Soc.* **127** 7941
[38] Abuabara S G, Rego L G C and Batista V S 2005 *J. Am. Chem. Soc.* **127** 18234
[39] Mou W, Hattori S, Rajak P, Shimojo F and Nakano A 2013 *Appl. Phys. Lett.* **102** 173301
[40] Duncan W R, Craig C F and Prezhdo O V 2007 *J. Am. Chem. Soc.* **129** 8528
[41] Li Z, Zhang X, Zhang Y, Woellner C F, Kuik M, Liu J, Nguyen T-Q and Lu G 2013 *J. Phys. Chem.* C **117** 6730
[42] Mikhnenko O V, Lin J, Shu Y, Anthony J E, Blom P W M, Nguyen T-Q and Loi M A 2012 *Phys. Chem. Chem. Phys.* **14** 14196
[43] Rim S-B, Fink R F, Schoneboom J C, Erk P and Peumans P 2007 *Appl. Phys. Lett.* **91** 173504
[44] Siebbeles L D A, Huijser A and Savenije T J 2009 *J. Mater. Chem.* **19** 6067
[45] Wei G, Lunt R R, Sun K, Wang S, Thompson M E and Forrest S R 2010 *Nano Lett.* **10** 3555
[46] Liu J, Mikhaylov I A, Zou J, Osaka I, Masunov A E, McCullough R D and Zhai L 2011 *Polymer* **52** 2302
[47] Ko S *et al* 2012 *J. Am. Chem. Soc.* **134** 5222
[48] Lap D V, Grebner D and Rentsch S 1997 *J. Phys. Chem.* A **101** 107
[49] Dias F B, Kamtekar K T, Cazati T, Williams G, Bryce M R and Monkman A P 2009 *ChemPhysChem* **10** 2096
[50] Scheblykin I G, Yartsev A, Pullerits T, Gulbinas V and Sundstrom V 2007 *J. Phys. Chem.* B **111** 6303
[51] Zhang X, Li Z and Lu G 2010 *Phys. Rev.* B **82** 205210
[52] Deng W Q and Goddard W A 2004 *J. Phys. Chem.* B **108** 8614
[53] Vukmirović N, Ponseca C S, Němec H, Yartsev A and Sundström V 2012 *J. Phys. Chem.* C **116** 19665
[54] Grozema F C and Siebbeles L D A 2008 *Int. Rev. Phys. Chem.* **27** 87
[55] Ulbricht R, Hendry E, Shan J, Heinz T F and Bonn M 2011 *Rev. Mod. Phys.* **83** 543
[56] Perdew J P, Burke K and Ernzerhof M 1996 *Phys. Rev. Lett.* **77** 3865
[57] Kresse G and Hafner J 1993 *Phys. Rev.* B **47** 558
[58] Kresse G and Furthmuller J 1996 *Phys. Rev.* B **54** 11169
[59] Zhang X, Li Z and Lu G 2012 *J. Phys.: Condens. Matter* **24** 205801
[60] Stein T, Eisenberg H, Kronik L and Baer R 2010 *Phys. Rev. Lett.* **105** 266802